Nonlinear Dynamics **22:** 393–413, 2000.

On the Design of the Piecewise Linear Vibration Absorber

D. PUN
Department of Civil Engineering, Hong Kong Polytechnic University, Kowloon, Hong Kong

Y. B. LIU
Institute of Mechanics, Chinese Academy of Science, Beijing 100080, P.R. China

(Received: 25 September 1997; accepted: 12 January 2000)

Abstract. This paper explores the potential of the piecewise linear vibration absorber in a system subject to narrow band harmonic loading. Such a spring is chosen because the design of linear springs is common knowledge among engineers. The two-degrees-of-freedom system is solved by using the Incremental Harmonic Balance method, and response aspects such as stiffness crossing frequency and jump behaviour are discussed. The effects of mass, stiffness, natural frequency ratios, and stiffness crossing positions on the suppression zone are probed. It is shown that a hardening absorber can deliver a wider bandwidth than a linear one over a range of frequencies. The absorber parameters needed to produce good designs have been determined and the quality of the realized suppression zone is discussed. Design guidelines are formulated to aid the parameter selection process.

Keywords: Piecewise linear, nonlinear, vibration, absorber.

1. Introduction

The vibration absorber has found extensive uses in engineering and there are continuing efforts to develop creative approaches to achieve better performance. This paper is concerned with the behaviour of the absorber under harmonic loading whose frequency varies over a narrow band, where it has been recognized that the employment of a nonlinear absorber spring can improve the operating frequency range. Specifically, the frequency response of a piecewise linear absorber is discussed in detail. The efficiency of an absorber in a narrow band environment is measured by the frequency window of a suppression band, within which the dynamic amplification of the structure displacement is less than one. Roberson [1] observed that, for the case of sinusoidal loading, an absorber with cubic springs can increase the bandwidth of the suppression zone over its linear counterpart. He further noted that a softening spring yields superior results over a hardening spring in the frequency range below the natural frequency of the structure. Arnold [2] studied a similar configuration and came to the interesting conclusion that a softening spring can have two anti-resonances, whereas a hardening spring has only one. Miller and Gartner [3] carried out theoretical and experimental work on a pneumatic spring absorber with hardening characteristics, and provided design details for a prototype.

Hunt and Nissen [4] analyzed a nonlinear absorber fabricated from softening Belleville springs under harmonic loading. They concluded that a bandwidth up to twice that of a linear spring can be obtained. Nissen et al. [5] conducted an optimization study on the application of the Belleville washer as an absorber spring and provided guidance on design.

Rice and McCraith [6] investigated an asymmetric Duffing-type nonlinear absorber for a structure subject to mass imbalance. They presented graphs on how the suppression bandwidth is affected by design parameters and showed results that are up to 50% better than the linear

absorber. They contended that a hardening absorber is equally as good as a softening one for maximizing the bandwidth.

Natsiavas [7, 8] analyzed an asymmetric piecewise linear absorber under a harmonic load. He assumed a single stiffness crossing per response cycle and obtained periodic solutions. For large stiffness change, he detected Hopf bifurcations, period doubling bifurcations, and chaotic motions. The focus was on bifurcation, chaos, and internal resonance, not the suppression zone.

Nissen et al. [5] provided a ready-to-use solution for the case of harmonic forcing by advocating the choice of softening Belleville washers. However, this arrangement is effective only for the situation where the excitation frequency is below the structure's natural frequency. The motivation for the present paper is to expand the arsenal of available devices by proposing the use of piecewise linear springs in absorber design.

The rationale for combining linear springs to achieve nonlinear behaviour is that engineers and designers are conversant with the design and fabrication of these components. The sizes and material types of these springs come in a wide range to accommodate the large spectrum of industrial and structural uses. Furthermore, the devices can be configured in a variety of ways, such as helical springs, tension springs, torsional springs, to suit the situation at hand. Of vital importance is that the design practices for these systems are common knowledge to engineers and are also easily accessible in reference works such as the one by the SAE Spring Committee [9]. This means that design, detailing and set-up of these assemblies can be completed in an expeditious and economical manner.

The objective of this paper is to demonstrate that a piecewise linear absorber under harmonic forcing can be effective in narrow band applications. It is shown that a hardening spring can substantially improve the bandwidth over that available from a simple linear spring over a reasonable frequency range.

The equations of motion for a two-degrees-of-freedom system representing a structure and an absorber are formulated in Section 2. The equations are solved using the Incremental Harmonic Balance method, as this is an accurate and efficient method for nonlinear frequency response. The method for stability analysis is presented in Section 3, for it is necessary to ensure that motion in the suppression zone is stable. The general behaviour of the system is illustrated in Section 4 in order to demonstrate the various modes of behaviour in different frequency regimes. The effects of various design parameters on the suppression band are investigated in detail in Section 5. Simple guidelines on the parameter selection process for achieving practical designs are discussed. Finally, the results are summarized and recommendations for future work are made in Section 6.

2. Formulation

The equation of motion for a two-degrees-of-freedom system shown in Figure 1 is

$$\begin{bmatrix} m_1 & 0 \\ 0 & m_2 \end{bmatrix} \begin{bmatrix} \ddot{y}_1 \\ \ddot{y}_2 \end{bmatrix} + \begin{bmatrix} c_1 + c_2 & -c_2 \\ -c_2 & c_2 \end{bmatrix} \begin{bmatrix} \dot{y}_1 \\ \dot{y}_2 \end{bmatrix} + \begin{bmatrix} k_1 y_1 - g(y_2 - y_1) \\ g(y_2 - y_1) \end{bmatrix} = \begin{bmatrix} p \cos \lambda t \\ 0 \end{bmatrix}, \quad (1)$$

where m_1, k_2, c_1, y_1 are the mass, stiffness, damping, and displacement, respectively, of the structure. The corresponding quantities for the absorber are denoted by the subscript 2, and the superscript $(\cdot)$ denotes differentiation with respect to time. The absorber stiffness comprises an initial branch k_2 and an extended branch k_d, connected at the stiffness crossing point e.

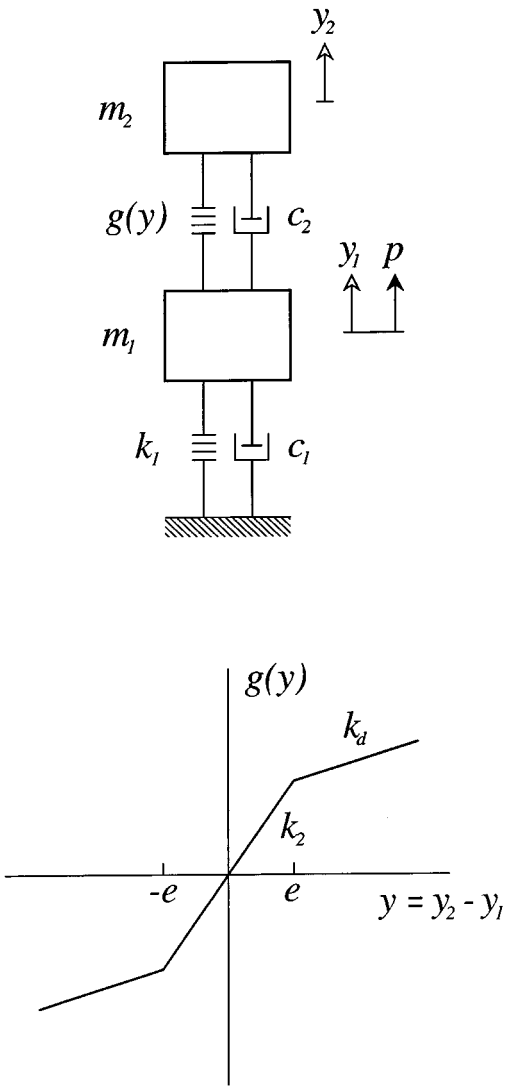

Figure 1. Structure and absorber model.

The applied harmonic load on the structure is p, the excitation frequency λ, and time t. The force-deflection relation $g(y)$ for the absorber spring, where y is the relative displacement, is

$$g(y_2 - y_1) = g(y) = \begin{cases} k_2 e + k_d(y - e), & y > e, \\ k_2 y, & -e \le y \le e, \\ -k_2 e + k_d(y + e), & y < -e. \end{cases} \tag{2}$$

A change of variable $\theta = \lambda t$ is introduced and Equation (1) is written in matrix form:

$$\lambda^2 \mathbf{M}\mathbf{y}'' + \lambda \mathbf{C}\mathbf{y}' + \mathbf{f}(\mathbf{y}) = \mathbf{p}(\theta), \tag{3}$$

where the primes denote differentiation with respect to θ. The Incremental Harmonic Balance (IHB) method is used to solve this equation, as this approach has been shown by Lau et al. [10] to be effective for finding periodic solutions for nonlinear vibration problems and has

been successfully applied in piecewise linear analysis by Pun et al. [11, 12]. The procedure here follows that of Lau and Zang [13]; a brief outline is described below, with more details in the Appendix.

Let the current motion be represented by $\mathbf{y}_0$ and λ_0, then the neighbouring states $\mathbf{y}$ and λ are given by

$$\mathbf{y} = \mathbf{y}_0 + \Delta\mathbf{y}, \quad \lambda = \lambda_0 + \Delta\lambda, \tag{4}$$

where Δ signifies an incremental change. Equation (3) is then expressed in incremental form by making use of Equation (4):

$$\lambda_0^2\mathbf{M}\Delta\mathbf{y}'' + \lambda_0\mathbf{C}\Delta\mathbf{y}' + \mathbf{S}\Delta\mathbf{y} = \boldsymbol{\varepsilon} + \mathbf{q}\Delta\lambda, \tag{5}$$

where $\mathbf{S}$ is the tangential stiffness matrix, $\boldsymbol{\varepsilon}$ is the residual force vector and equals $\mathbf{0}$ if the current solution is correct, and $\mathbf{q}$ is the force vector due to a unit frequency change. The periodic solution is taken as

$$y_i = \sum_{i=1}^{n}(a_{ij}\cos j\theta + b_{ij}\sin j\theta) \quad (i = 1 \ldots 2), \tag{6}$$

where n is the number of harmonic terms, a_{ij} and b_{ij} are the amplitudes of the cosine and sine harmonics, respectively. Let

$$\mathbf{z} = [a_{1j}, \ldots, b_{1j}, \ldots, a_{2j}, \ldots, b_{2j}, \ldots]^T \quad (j = 1 \ldots n), \tag{7}$$

then

$$\mathbf{y} = \mathbf{H}\mathbf{z}. \tag{8}$$

Substituting Equation (8) into Equation (5), and then performing the Galerkin procedure yields

$$\mathbf{A}\Delta\mathbf{z} = \bar{\boldsymbol{\varepsilon}} + \bar{\mathbf{q}}\Delta\lambda. \tag{9}$$

The matrices $\mathbf{S}$, $\mathbf{H}$, $\mathbf{A}$, $\boldsymbol{\varepsilon}$, $\bar{\boldsymbol{\varepsilon}}$, $\mathbf{q}$, $\bar{\mathbf{q}}$ are given in the Appendix. It is noted that the integrals in the Galerkin step necessitate the determination of the stiffness regimes of the absorber, which are obtained by solving the values of θ, for which

$$y_2 - y_1 = e \quad \text{or} \quad y_2 - y_1 = -e, \tag{10}$$

by considering Equation (6). These angles are the temporal transition points between the stiffness branches and can be ordered to delimit the motion status.

The solution process can be started by using estimated amplitudes at a prescribed frequency, which means that λ is fixed and $\Delta\lambda = 0$. Equation (9) is then iterated for $\Delta\mathbf{z}$ until $\bar{\boldsymbol{\varepsilon}}$ becomes acceptably small, indicating that a correct solution has been attained. The solution at a neighbouring frequency value is next sought by using the previously found $\mathbf{z}$ as a starting point, prescribing $\Delta\lambda$ and repeating the iteration procedure. In this way the entire resonance curve can be traced out. A more complete discussion on the continuation strategy is contained in [14].

3. Stability Analysis

The approach to stability analysis is based on that introduced by Masri and Caughey [15] and the procedure follows the formulation outlined in Pun et al. [16]. To facilitate analysis, the equation of motion is expressed in standard state-space form:

$$\mathbf{D}\dot{\mathbf{v}} + \mathbf{G}\mathbf{v} = \mathbf{p_d}\cos(\lambda t + \phi) + \mathbf{p_s}, \tag{11}$$

$$\mathbf{v} = [\dot{y}_1, \dot{y}_2, y_1, y_2]^T. \tag{12}$$

(The details for these and the following matrices are provided in the Appendix.) This equation is valid within a single stiffness regime, and the phase angle ϕ is introduced to maintain force continuity in the piecewise linear nature of the motion.

The solution to Equation (11) can be written as

$$\mathbf{v} = \mathbf{B}\mathbf{E}(t)\mathbf{B}^{-1}(\mathbf{v}_0 - \boldsymbol{\mu}_0\boldsymbol{\phi} - \mathbf{v}_s) + \boldsymbol{\mu}(t)\boldsymbol{\phi} + \mathbf{v}_s, \tag{13}$$

$$\mathbf{v}_0 = [\dot{y}_1(0), \dot{y}_2(0), y_1(0), y_2(0)]^T, \tag{14}$$

where the motion begins at a stiffness boundary, as governed by Equation (10), and the starting time is 0. The perturbed motion $\tilde{\mathbf{v}}$ caused by deviation in the initial conditions is

$$\tilde{\mathbf{v}} = \mathbf{v} + \delta\mathbf{v}. \tag{15}$$

The motion deviation $\delta\mathbf{v}$ can be expressed as

$$\delta\mathbf{v}(t + \delta t) = \frac{\partial\mathbf{v}}{\partial\mathbf{v}_0}\delta\mathbf{v}_0 + \frac{\partial\mathbf{v}}{\partial\phi}\delta\phi + \frac{\partial\mathbf{v}}{\partial t}\delta t. \tag{16}$$

Making use of Equation (13) in Equation (16) results in

$$\begin{aligned}\delta\mathbf{v}(t + \delta t) \;=\; & \mathbf{B}\mathbf{E}(t)\mathbf{B}^{-1}\delta\mathbf{v}_0 - \mathbf{B}\mathbf{E}(t)\mathbf{B}^{-1}\boldsymbol{\mu}_0\bar{\boldsymbol{\phi}}\delta\phi \\ & + \boldsymbol{\mu}(t)\bar{\boldsymbol{\phi}}\delta\phi + \mathbf{B}\dot{\mathbf{E}}(t)\mathbf{B}^{-1}\bar{\mathbf{v}}_0\delta t + \dot{\boldsymbol{\mu}}(t)\boldsymbol{\phi}\delta t,\end{aligned} \tag{17}$$

$$\bar{\mathbf{v}}_0 = \mathbf{v}_0 - \boldsymbol{\mu}_0\boldsymbol{\phi} - \mathbf{v}_s. \tag{18}$$

As the flight regions are determined by the relative displacement y, δy is used instead of δy_2 by transforming $\delta\mathbf{v}$ to $\delta\mathbf{w}$

$$\delta\mathbf{w} = \mathbf{T}\delta\mathbf{v}, \tag{19}$$

$$\delta\mathbf{w} = [\delta\dot{y}_1, \delta\dot{y}, \delta y_1, \delta y]^T, \tag{20}$$

$$\delta\mathbf{w}_0 = [\delta\dot{y}_1(0), \delta\dot{y}(0), \delta y_1(0), \delta y(0)]^T, \tag{21}$$

$$\begin{aligned}\delta\mathbf{w}(t + \delta t) \;=\; & \mathbf{T}\mathbf{B}\mathbf{E}(t)\mathbf{B}^{-1}\mathbf{T}^{-1}\delta\mathbf{w}_0 - \mathbf{T}\mathbf{B}\mathbf{E}(t)\mathbf{B}^{-1}\boldsymbol{\mu}_0\bar{\boldsymbol{\phi}}\delta\phi + \mathbf{T}\boldsymbol{\mu}(t)\bar{\boldsymbol{\phi}}\delta\phi \\ & + \mathbf{T}\mathbf{B}\dot{\mathbf{E}}(t)\mathbf{B}^{-1}\bar{\mathbf{v}}_0\delta t + \mathbf{T}\dot{\boldsymbol{\mu}}(t)\boldsymbol{\phi}\delta t.\end{aligned} \tag{22}$$

To retain the perturbed motion along the stiffness boundary at $t = 0$, $\delta y(0)$ is taken as 0 and the phase angle is perturbed through $\delta\phi$. The original motion reaches the next stiffness boundary

at $t = t_1$, but the perturbed motion arrives at this point at a slightly different time $t_1 + \delta t$, when δy becomes 0. These observations can be utilized in the fourth row of Equation (22) to obtain a relation for δt:

$$0 = \sum_{j=1}^{3} [\mathbf{TBE}(t_1)\mathbf{B}^{-1}\mathbf{T}^{-1}]_{4j}[\delta \mathbf{w}_0]_j + [-\mathbf{TBE}(t_1)\mathbf{B}^{-1}\boldsymbol{\mu}_0\bar{\boldsymbol{\phi}} + \mathbf{T}\boldsymbol{\mu}(t_1)\bar{\boldsymbol{\phi}}]_4\delta\phi + [\mathbf{TB}\dot{\mathbf{E}}(t_1)\mathbf{B}^{-1}\bar{\mathbf{v}}_0 + \mathbf{T}\dot{\boldsymbol{\mu}}(t_1)\boldsymbol{\phi}]_4\delta t, \tag{23}$$

where the subscripts of the brackets refer to the elements of the enclosed matrix or vector. Furthermore, consideration of the continuity of the harmonic force yields

$$\delta\phi(t + \delta t) = \lambda\delta t + \delta\phi. \tag{24}$$

The δy term in $\delta \mathbf{w}$ is replaced by $\delta\phi$ to form $\delta\bar{\mathbf{w}}$ as the appropriate motion deviation. This is achieved by combining the first three rows of Equations (22), (23) and (24) to give

$$\delta\bar{\mathbf{w}}_1 = \mathbf{Q}_1\delta\bar{\mathbf{w}}_0, \tag{25}$$

$$\delta\bar{\mathbf{w}}_0 = [\delta\dot{y}_1(0), \delta\dot{y}(0), \delta y_1(0), \delta\phi]^T, \tag{26}$$

where $\delta\bar{\mathbf{w}}_0$ and $\delta\bar{\mathbf{w}}_1$ are the deviations at the beginning and end of this flight leg, respectively. This analysis is then repeated for the next flight regime, using $\delta\bar{\mathbf{w}}_1$ as the initial deviation. As there are four stiffness crossings in a period, the deviation $\delta\bar{\mathbf{w}}_4$ at the end of a period is given by

$$\delta\bar{\mathbf{w}}_4 = \mathbf{Q}_4\mathbf{Q}_3\mathbf{Q}_2\mathbf{Q}_1\delta\bar{\mathbf{w}}_0 = \mathbf{Q}\delta\bar{\mathbf{w}}_0. \tag{27}$$

The initial conditions $\mathbf{v}_0$ and the stiffness crossing times t_i ($i = 1 \ldots 4$) are available from the IHB solution, so that $\mathbf{Q}$ can be readily calculated. The eigenvalues of $\mathbf{Q}$ determine whether the deviation grows or decays with time. The interest here is in a stable periodic orbit and the modulus of every eigenvalue should be less than 1.

4. Fundamental Behaviour

The uncoupled natural frequencies w_1 and w_2, together with the following normalized variables, are introduced:

$$\begin{aligned}
w_1 &= \sqrt{\frac{k_1}{m_1}}, \quad w_2 = \sqrt{\frac{k_2}{m_2}}, \\
x_1 &= \frac{k_1 y_1}{p}, \quad x_2 = \frac{k_1 y_2}{p}, \\
d_1 &= \frac{c_1}{2\sqrt{k_1 m_1}}, \quad d_2 = \frac{c_2}{2\sqrt{k_2 m_2}}, \\
m &= \frac{m_2}{m_1}, \quad r = \frac{w_2}{w_1}, \quad \alpha = \frac{\lambda}{w_1}, \\
k &= \frac{k_d}{k_2}, \quad u = \frac{k_1 e}{p}, \quad v = \frac{1}{mr^2},
\end{aligned} \tag{28}$$

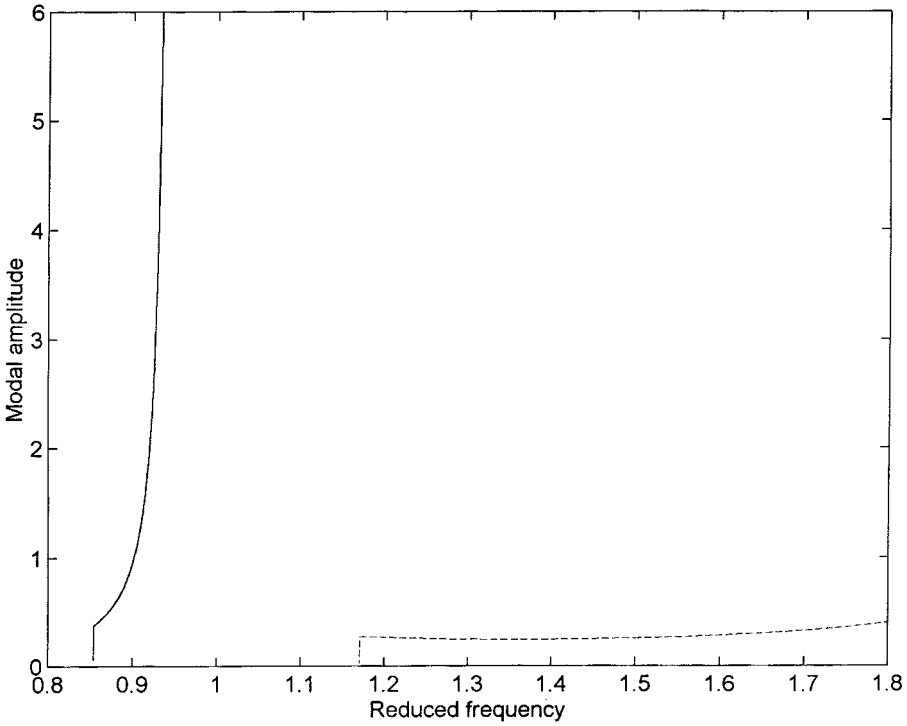

Figure 2. Free vibration modes, reduced displacement *versus* reduced frequency, case 1, — mode 1, - - - mode 2.

where x_i is the reduced displacement, d_i the damping ratio, m the mass ratio, r the natural frequency ratio, k the stiffness ratio, u the stiffness crossing position, α the reduced frequency, and the subscripts 1 and 2 refer to the structure and absorber, respectively. The stiffness crossing position u is a displacement measure of the nonlinear strength and should be seen as being relative to the displacement v of a linear undamped absorber excited at the natural frequency ratio r. This is the linear turning frequency at which the structure is stationary because the absorber can completely counterbalance the applied force. If u is larger than v, then nonlinear action does not occur because linear action alone can cancel the loading. If u is less than v, then nonlinear action is precipitated as the absorber moves beyond u to reach dynamic equilibrium.

In this section the general behaviour of the piecewise linear absorber is illustrated through representative cases that reflect the various modes of response. The basic parameters are a mass ratio of 0.1, natural frequency ratio of 1, structure damping ratio of 0.05, and absorber damping ratio of 0.01. The stiffness ratio and crossing position are varied as follows: (1) $k = 4$, $u = 1$; and (2) $k = 2$, $u = 1$. The structure damping ratio has little effect on the suppression zone and the chosen value is simply a reasonable figure. The absorber damping does influence the results and a minimum value following Nissen et al. [5] is used. Case 1 is a highly nonlinear hardening absorber, whereas case 2 is a low nonlinear strength absorber. The two system normalized (with respect to w_1) natural frequencies in both cases are 0.8542 and 1.1705. Three harmonic terms have been used to compute the following response.

The free vibration backbone curves for the system in case 1 are shown in Figure 2. The fundamental backbone curve grows more rapidly than that at the second frequency, which is bent considerably more to the right. This is a sign that nonlinear behaviour is more pronounced

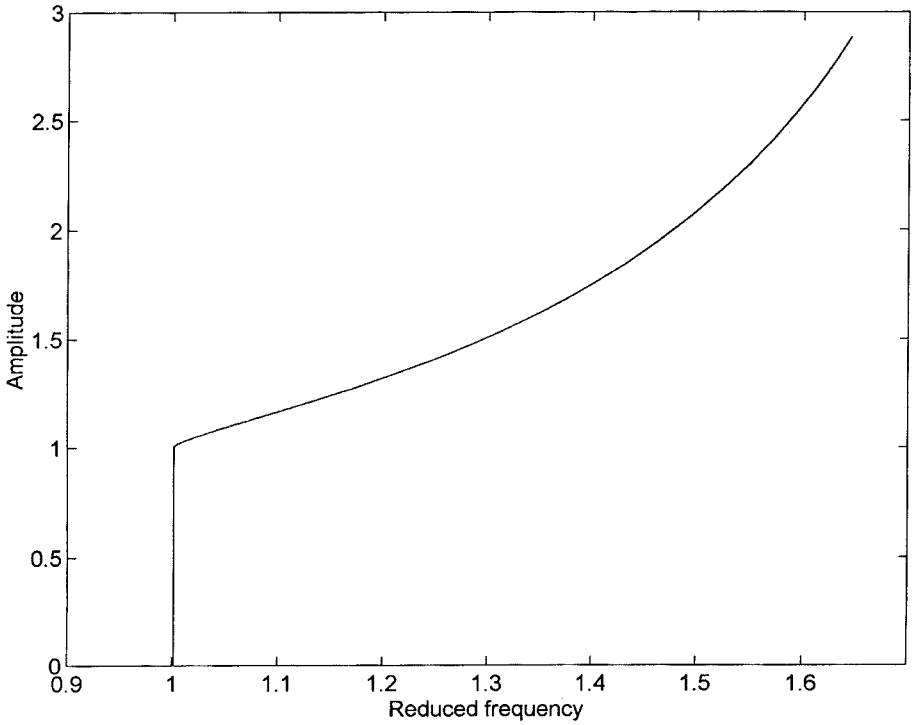

Figure 3. Backbone curve of the absorber alone, reduced displacement *versus* reduced frequency, case 1.

at the second natural frequency. This characteristic is intimately related to the free vibration behaviour of the absorber as a single-degree-of-freedom oscillator. The free vibration backbone curve of the absorber spring alone is shown in Figure 3 and, as it is a hardening spring, the curve leans towards the increasing frequency direction. This is the reason why the composite system second mode exhibits a considerable nonlinear quality.

The forced responses around the suppression zone for the structure and absorber are shown in Figures 4 and 5. The structure looping response around the reduced frequency of 2 is caused by the hysteresis of the absorber. As the hysteresis is proportional to the nonlinearity, the extent of the looping response is a function of the nonlinear strength of the absorber. It is known that hysteresis in an oscillator can be controlled by damping, and in the light of the connection between the absorber oscillator and the structure, it is apparent that absorber damping is fruitful for diminishing the structure looping response. However, the use of absorber damping is always a dilemma because it reduces absorber displacements and, hence, lowers absorber efficiency.

For a structure under harmonic loading, the vibration of the absorber mass exerts a force in the absorber spring to counteract the applied force, thus minimizing the displacement of the main mass. For a linear absorber whose backbone curve is a vertical straight line at the natural frequency ratio, the suppression zone is positioned at that frequency. For a hardening absorber with a backbone curve bent to the right, it follows that the suppression zone is located to the right of the natural frequency ratio.

Natsiavas [7, 8] solved periodic solutions by using an analytical procedure formulated on the basis of a single stiffness crossing for an asymmetric piecewise linear absorber. Accounting for the differences in stiffness symmetry and the starting reference position, that is

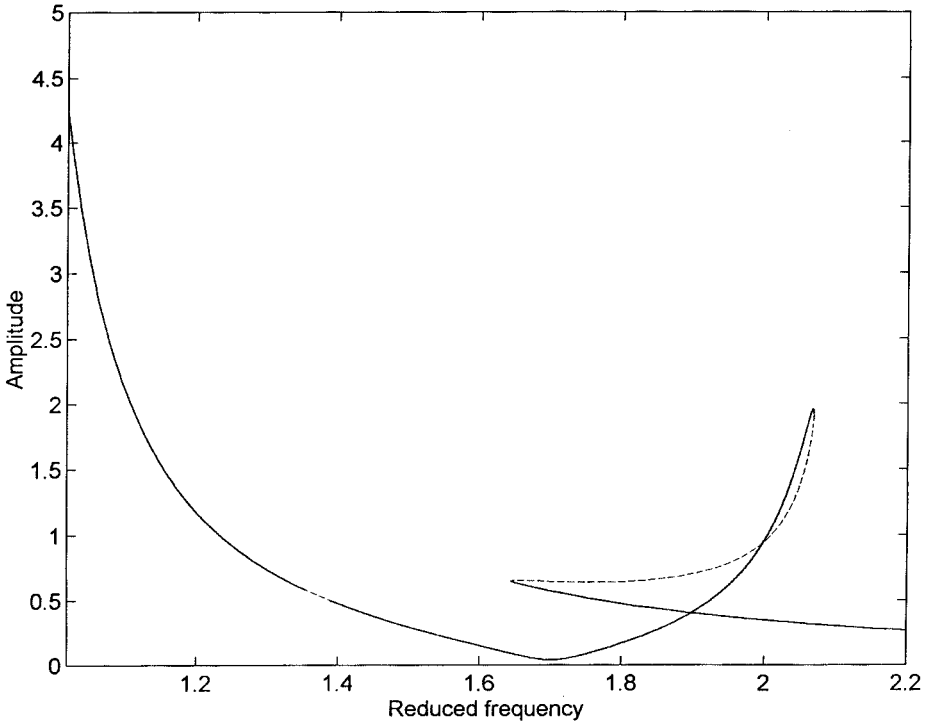

Figure 4. Structure's reduced displacement *versus* reduced frequency, forced vibration, case 1, — stable, - - - unstable.

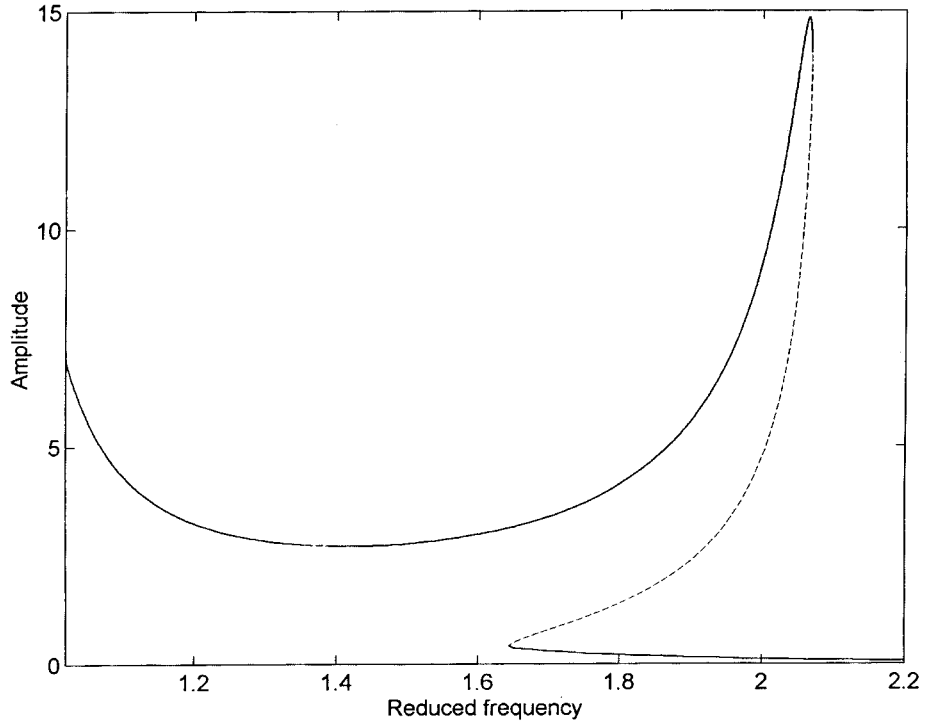

Figure 5. Absorber's reduced displacement *versus* reduced frequency, forced vibration, case 1, — stable, - - - unstable.

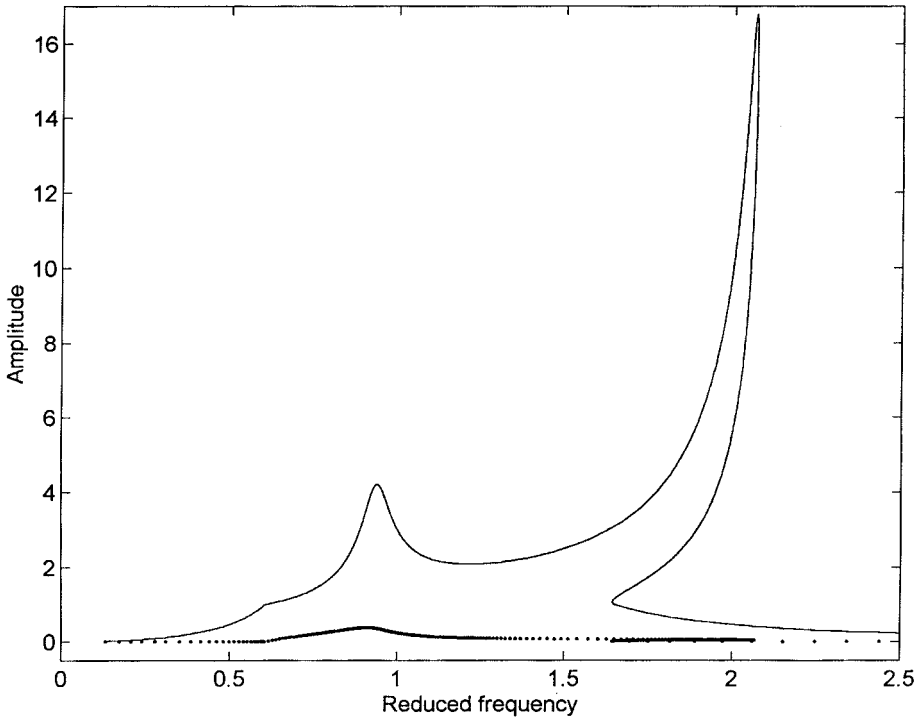

Figure 6. Absorber's relative reduced displacement *versus* reduced frequency, forced vibration, case 1, — first harmonic, - - - second harmonic.

equivalent to a four stiffness crossing in the present case. As it is not necessary to make an assumption concerning the crossing frequency in utilizing the IHB method, it is instructive to examine the current results from this perspective. The IHB analysis has been carried out with three odd harmonics, and the magnitudes of the first and second harmonics of the absorber's relative reduced displacement are plotted in Figure 6, from which it is apparent that the second harmonic is a small fraction of the first for the complete frequency range. The third harmonic is not shown as it is generally very close to 0. It can be seen that the second harmonic is nearly 0 in the reduced frequency regime of 1.2 to 2 where the suppression zone is located. Motions dominated by the first harmonic show four crossings per cycle, as higher harmonics are needed to supply the higher frequency components that lead to more crossings. The time history of the motion at a reduced frequency of 0.78, where the amplitude of the second harmonic is maximum, is presented in Figure 7. There are four stiffness crossings per period, which is a typical scenario. This result is a confirmation that there are generally four stiffness crossings per cycle for the stiffness range appropriate for absorber springs.

Figure 4 shows that the structure response traces out a loop inside the suppression zone, an obviously undesirable feature due to the presence of the jump phenomenon, which can lead to volatile motion. This is attributed to strong nonlinearity in the form of a high stiffness ratio. It is more usual to see a loop overhanging the zone rather than directly within it as here. However, such an encroachment still presents the possibility of highly abrupt movement, where the periodic solution jumps from one branch to another, should the structure be subject to an accidental displacement. Furthermore, high nonlinearity may induce bifurcations in the suppression zone, where unstable periodic response yields to quasi-periodic motion, as de-

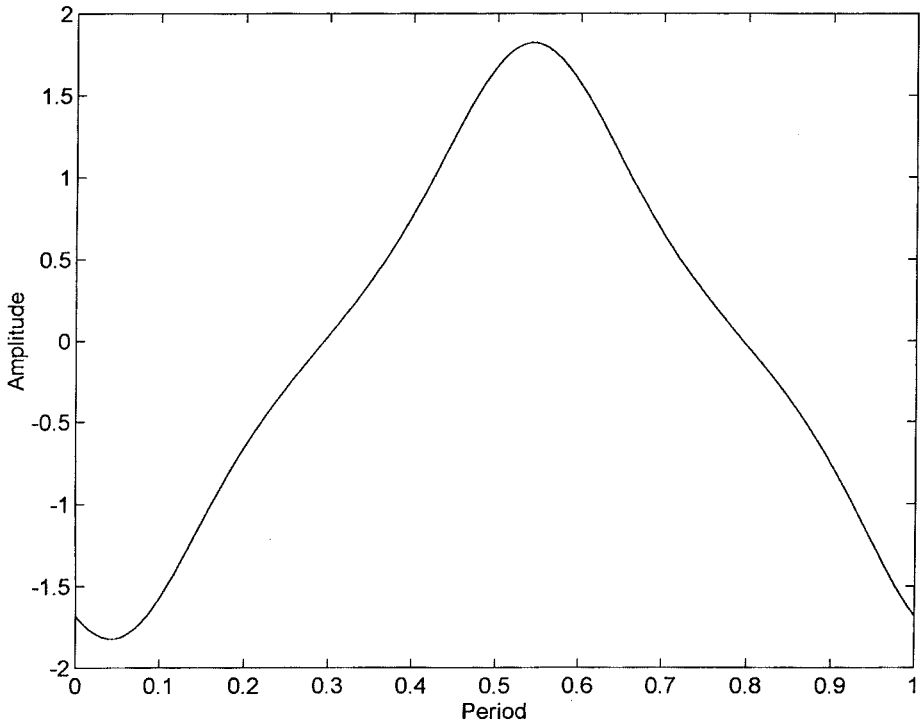

Figure 7. Time history of structure's reduced displacement, forced vibration, case 1, $\alpha = 0.78$.

tailed in Rice and McCraith [6], and Natsiavas [7, 8]. This is evident at the reduced frequency of 1.37, where Hopf bifurcations caused by excessive nonlinearity are detrimental to absorber performance.

The frequency response of the structure in case 2, a weakly hardening absorber, is shown in Figure 8. It can be seen that there is no loop in the response and all the solutions are stable. This is due to the low nonlinearity of the system, and certainly the quality of the motion around the suppression zone is better than the previous case.

5. Suppression Zone Analysis

In this section the effects of the stiffness ratio, crossing position, and natural frequency ratio on the characteristics of the suppression band are investigated in some detail. It is well known that the band increases with mass ratio and, hence, two representative values of this parameter, 0.25 and 0.1, are used for illustration. The structure and absorber damping ratios are fixed at 0.05 and 0.01, respectively, as in the previous section. In this work it has been found that structure damping has very little effect on the zone. Three harmonic terms have been used to compute the following results.

The suppression zone boundaries for a system with a mass ratio of 0.25, natural frequency ratio of 1, and a tuned linear absorber displacement of 4, are plotted as a function of the stiffness ratio in Figure 9. Two cases are considered, one with a crossing position 1 and the other 4. The boundaries converge at the stiffness ratio of 1 because the system becomes linear at this point and, thus, the influence of nonlinearity is brought out in the diagram. For a crossing position of 4, the zone abruptly widens for stiffness ratios below 0.2, and in contrast

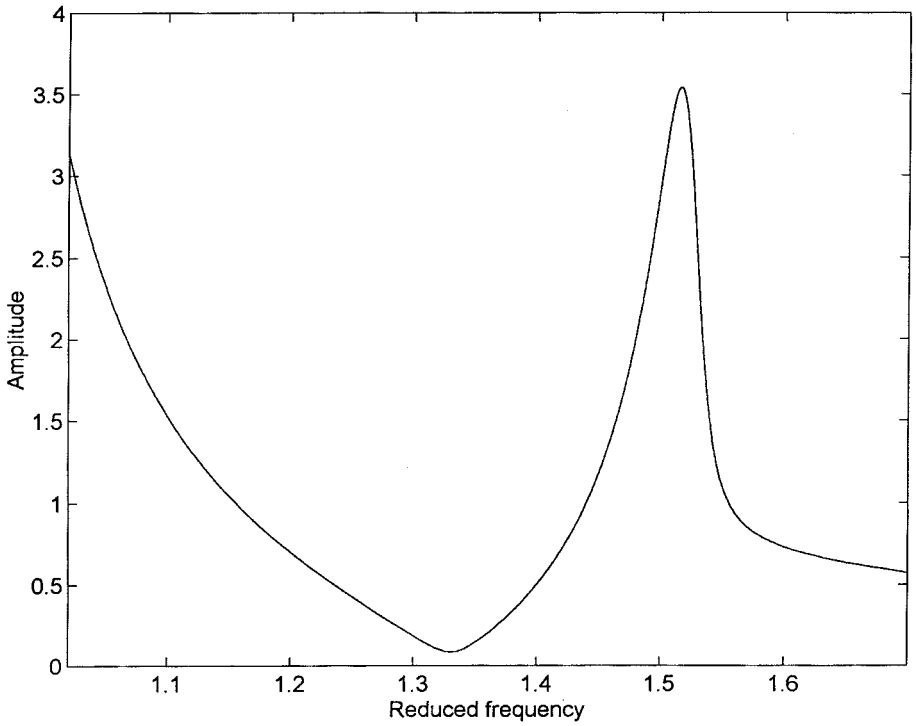

Figure 8. Structure's reduced displacement *versus* reduced frequency, forced vibration, case 2, — stable.

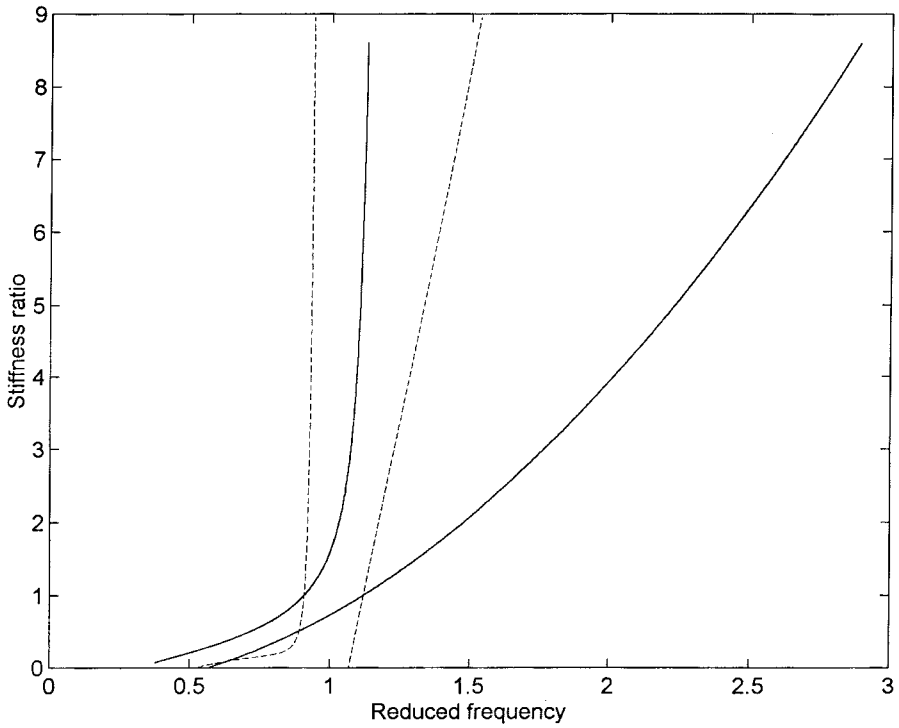

Figure 9. Suppression zone boundaries, stiffness ratio *versus* reduced frequency, $m = 0.25$, — $u = 1$, - - - $u = 4$.

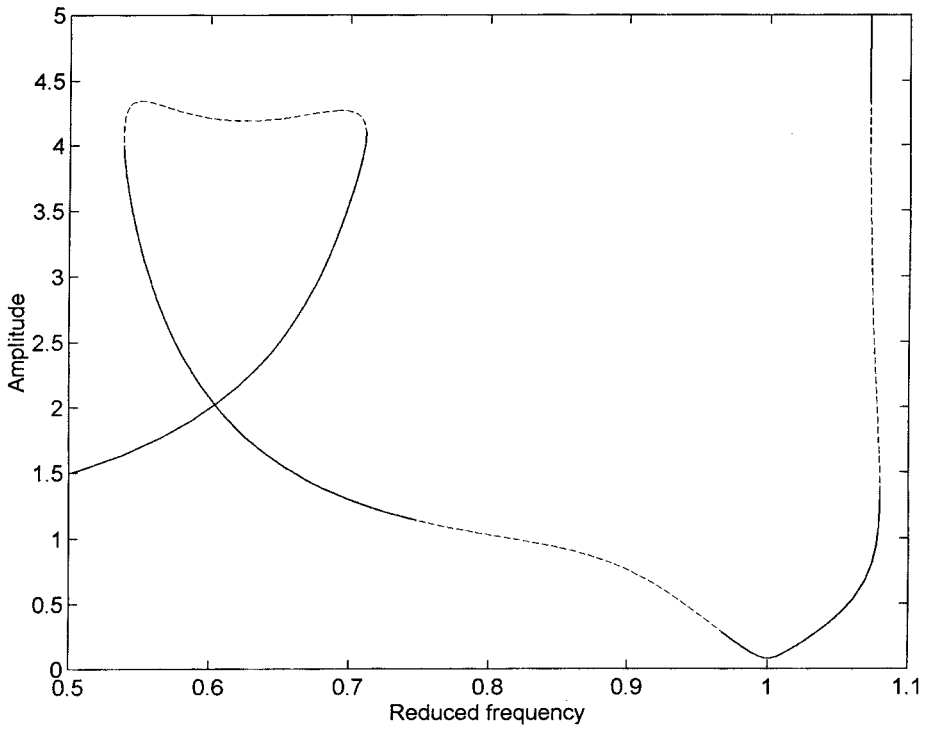

Figure 10. Structure's reduced displacement *versus* reduced frequency, $m = 0.25$, $k = 0.2$, $u = 4$, — stable, - - - unstable.

it widens only marginally for higher stiffness ratios. The opposite behaviour is observed for a crossing position of 1, where the zone widens for high stiffness ratios but narrows for low ones. Unfortunately, the solutions in the low stiffness ratio region for a crossing position of 4 are not stable, as shown in Figure 10 for a stiffness ratio of 0.2. However, the crossing position 1 case can be realized in practice, as Figure 11 shows that the solutions in the zone are able for a stiffness ratio of 2. The equivalent linear absorber is that with a stiffness ratio of 1 in Figure 9. It can be seen that the nonlinear absorber produces a bandwidth of 0.35, compared with the linear case of 0.21, an improvement of 1.7 times.

The variation of the zone as a function of the crossing position is shown more directly in Figure 12. For a natural frequency ratio of 1 (stiffness ratio of 2), it is apparent that the bandwidth increases with a decreasing crossing position. Next, the effect of the natural frequency ratio, is illustrated, and Figure 13 shows that for a crossing position of 1 (stiffness ratio of 2) lowering the natural frequency ratio below 1 decreases the bandwidth. For convenience, the absorber damping ratio has been kept at 0 for the analyses in this figure, as checks show that the results are nearly identical to those for a damping of 0.01. These results and other similar ones have shown that, for effective bandwidth control, changes in one variable need to be compensated by variations in others to lead to a sound performance.

For the low mass ratio case of 0.1, the suppression zone boundaries are shown in Figure 14 for a natural frequency ratio of 1, tuned linear absorber displacement of 10, with crossing positions 1 and 10. The same general behaviour as for the heavy mass ratio case is exhibited and it is seen that a hardening absorber with a stiffness ratio of 2 and crossing position of 1 is effective in providing a good bandwidth. The zone ranges from a reduced frequency of

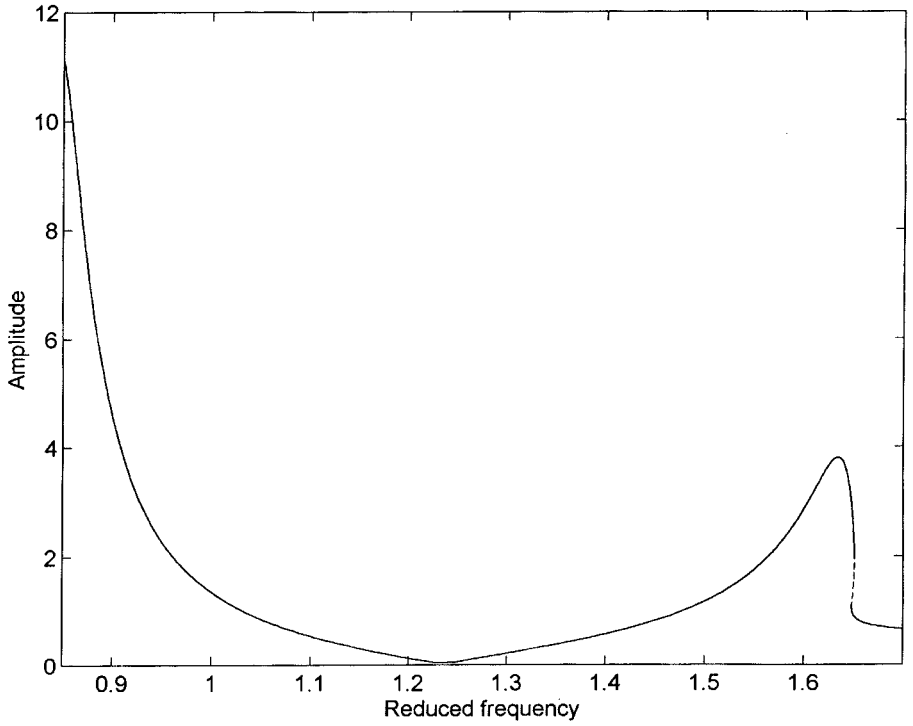

Figure 11. Structure's reduced displacement *versus* reduced frequency, $m = 0.25$, $k = 2$, $u = 1$, — stable, - - - unstable.

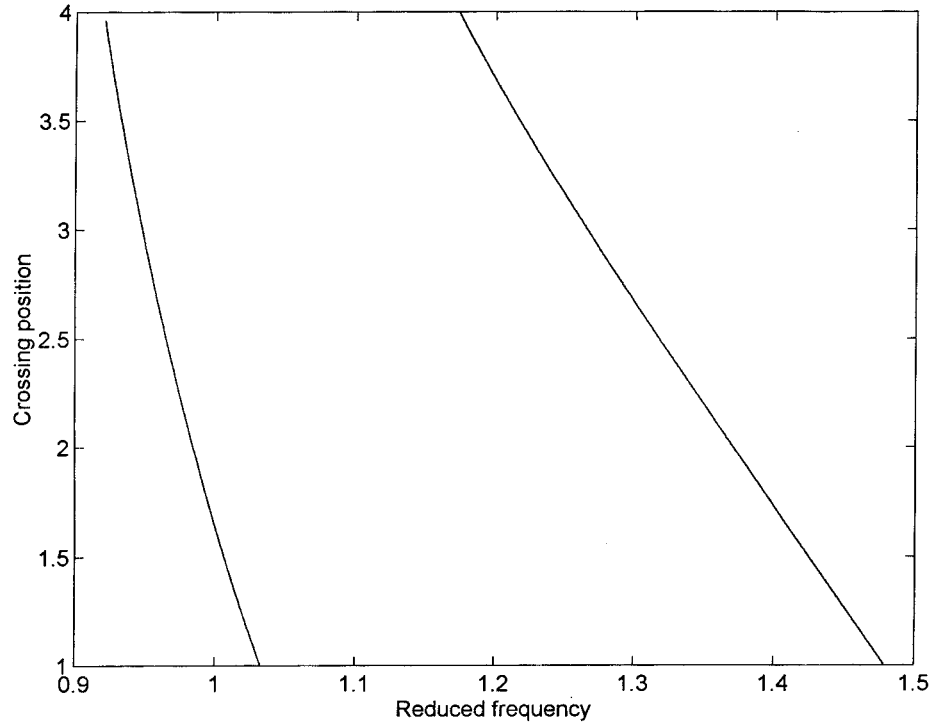

Figure 12. Suppression zone boundaries, crossing position *versus* reduced frequency, $m = 0.25$, $k = 2$.

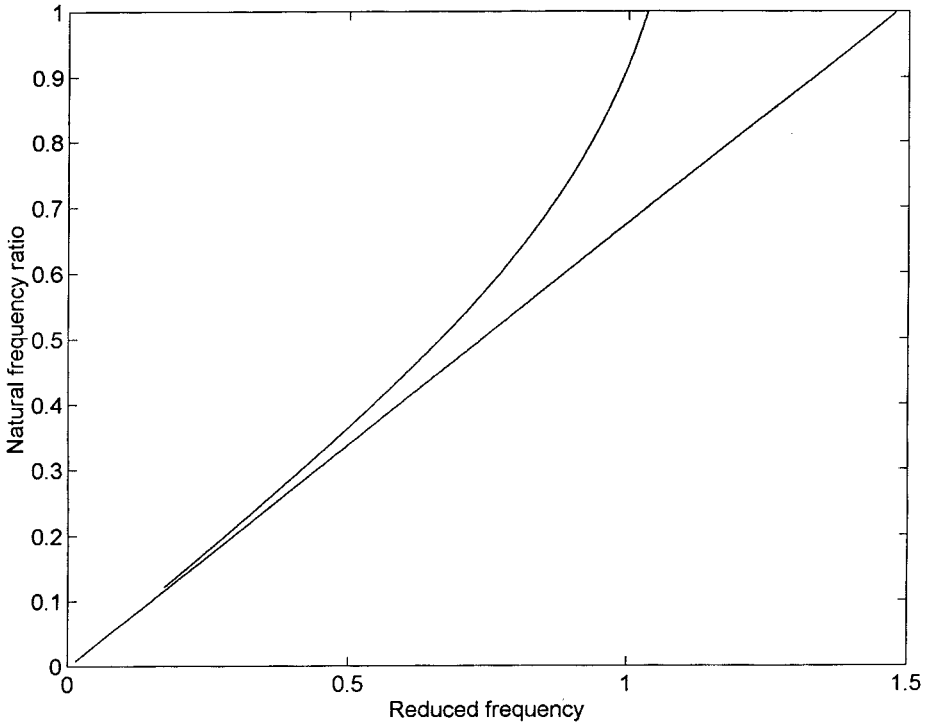

Figure 13. Suppression zone boundaries, natural frequency ratio *versus* reduced frequency, $m = 0.25$, $k = 2$, $u = 1$.

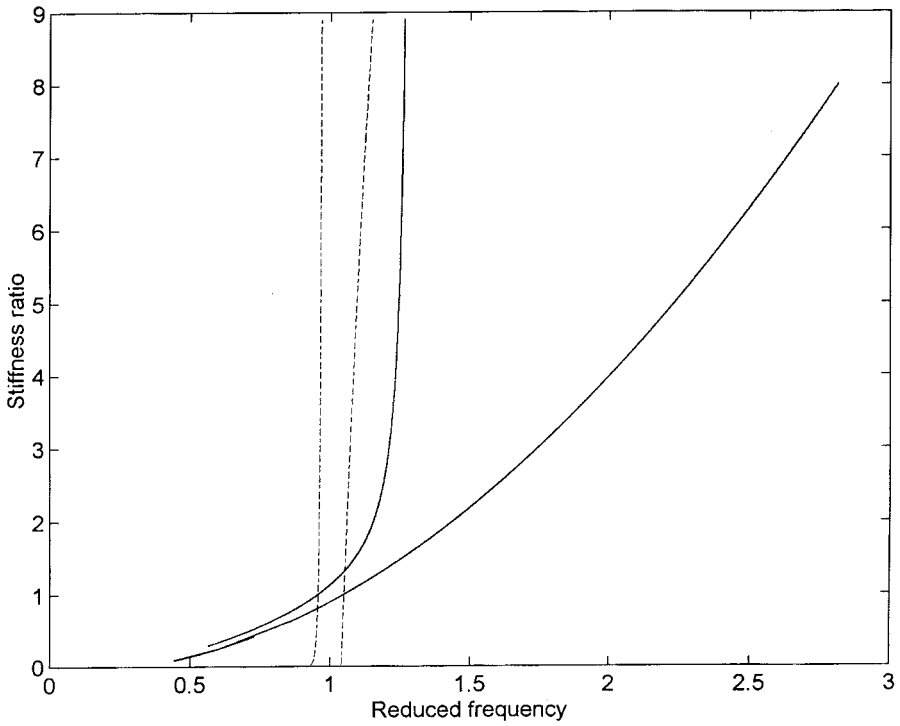

Figure 14. Suppression zone boundaries, stiffness ratio *versus* reduced frequency, $m = 0.1$, — $u = 1$, - - - $u = 10$.

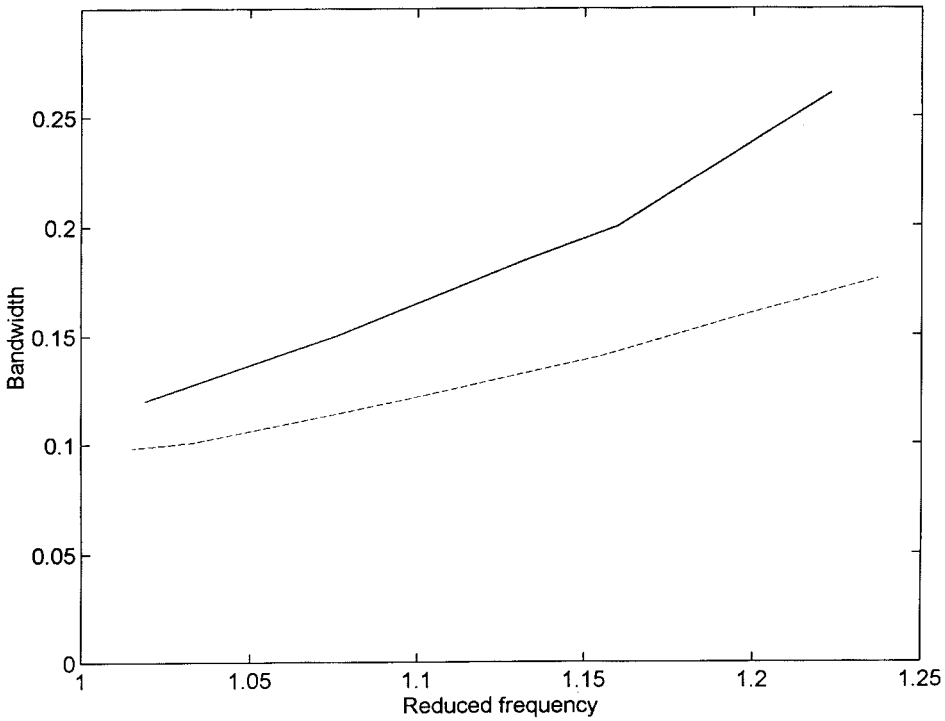

Figure 15. Bandwidth *versus* trough's reduced frequency, — nonlinear, - - - linear.

1.15 to 1.44, for a bandwidth of 0.29 which is a 3.2 times improvement over the linear case of 0.09. This enhancement is better than that for the heavier mass ratio of 0.25, where the increase is only 1.7 times for the same stiffness ratio. This is achieved at the expense of higher nonlinearity in terms of the crossing position, which results in shifting the zone slightly to the right. The resonance curve for this case has already been shown in Figure 8, where periodic solutions in the zone are stable. An absorber with a crossing position of 10 is not effective, even at very low values of stiffness ratio.

The paradigm that a hardening absorber can provide good bandwidth at a low stiffness crossing position serves as a starting point in the search for appropriate absorber configurations. The frequency at which the minimum displacement in the zone occurs is used as a reference, and is referred to as the trough frequency. For a mass ratio of 0.1, extensive analysis on absorber performance has yielded a relationship between the bandwidth and the trough's reduced frequency which is presented in Figure 15. The corresponding values for a linear absorber are also plotted. It is evident that the bandwidth increases as the zone moves away from the region near the structure frequency.

The benefit of a piecewise linear absorber can be illustrated in an example. Consider a structure of mass 10 kg, support stiffness 28000 N/m, damping 52.92 N-sec/m, resulting in a natural frequency of 52.92 rad/sec. A harmonic load of magnitude 700 N acts on the structure at an operating frequency of 62.83 rad/sec. A linear absorber tuned to the operating frequency with mass 1 kg, stiffness 3947.77 N/m, damping 1.26 N-sec/m, corresponding to $m = 0.1$ and $d_2 = 0.01$, gives a suppression zone from 57.9 to 65.95 rad/sec, for a bandwidth of 8.05 rad/sec. A piecewise linear absorber of the same mass, initial stiffness 1792 N/m, extended stiffness 4838.4 N/m, stiffness crossing point 0.0375 m, damping 0.85 N-sec/m,

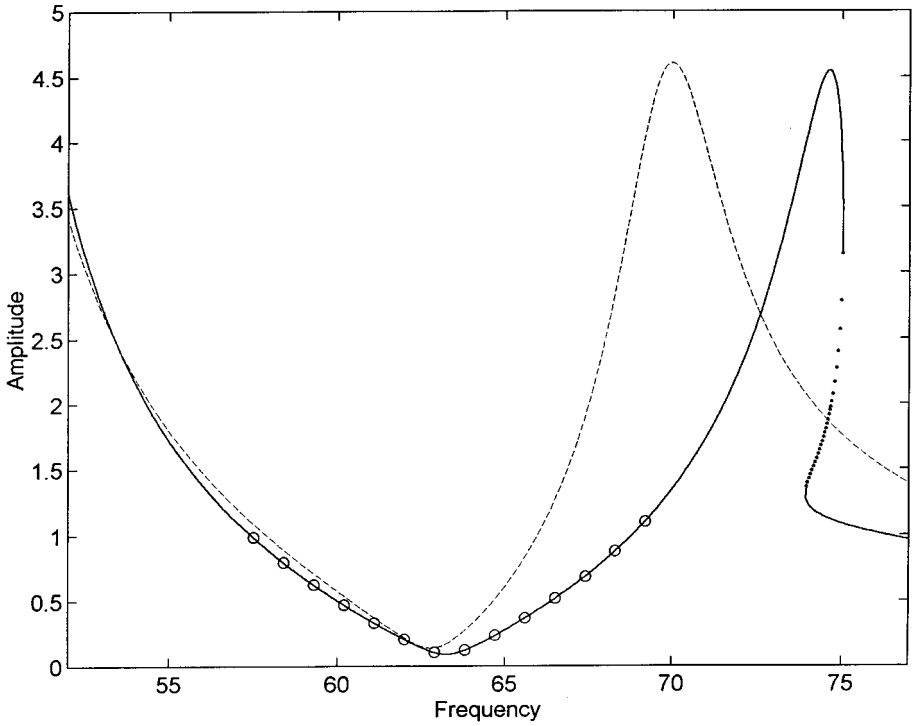

Figure 16. Structure's reduced displacement *versus* frequency, — (· · ·) nonlinear stable (unstable), – – linear, ○ ○ ○ time integration.

provides a zone from 57.44 to 68.84 rad/sec, for a bandwidth of 11.4 rad/sec. This zone is 41% wider than the linear one. The trough frequency is at 63.27 rad/sec which is almost identical to the operating frequency. This case corresponds to $m = 0.1$, $r = 0.8$, $k = 2.7$, $u = 1.5$, $v = 15.6$, $d_1 = 0.05$, $d_2 = 0.01$. The bandwidth and trough frequency can be normalized by the structure's natural frequency to give reduced values of 0.22 and 1.19, respectively, which are in agreement with Figure 15. The suppression zones given by the nonlinear absorber, linear absorber, and time integration results for the nonlinear case are compared in Figure 16. Note that the nonlinear absorber yields an almost symmetric zone with gentle slopes along the sides, so that the displacement does not increase steeply once the excitation sways beyond the borders.

Some design guidelines can be formulated on the basis of the above results. It can be seen from Figure 11 that increasing the stiffness ratio while keeping other parameters constant increases the bandwidth, and moves the suppression zone to the right. Also apparent from the same diagram is that lowering the stiffness crossing has a similar effect. Figure 15 shows that the bandwidth increases as the natural frequency ratio is raised. These three fundamental aspects can be used to configure an absorber for top response, in conjunction with the following suggested parameter ranges. The stiffness ratio should be between 2 and 3, as higher values generally lead to instability problems in the zone. The stiffness crossing position, which accounts for both the load magnitude and the mass ratio, should be between 0.1 and 0.25 of the tuned absorber displacement. The desired trough frequency determines the natural frequency ratio, which should be about 0.6 to 0.9 of the former. This is to enable the formation of a symmetric zone, so as to allow movement of the operating frequency in both directions.

Having established the preliminary parameters, these can then be fine tuned according to the three basic guidelines. For instance, if the trough frequency turns out to be lower than anticipated, then increasing the stiffness ratio or the natural frequency ratio, or lowering the crossing position, are choices of action that can improve the situation. Another scenario may be that the trough frequency is correct but the bandwidth is too narrow. A possible way to rectify this is to lower both the natural frequency ratio and the crossing position, and to increase the stiffness ratio. The present results indicate that there are usually more than one configuration that can yield a good bandwidth at a particular frequency. This means that there are various combinations of the parameters that can develop very similar suppression zones, on account of the interaction among the principal parameters as explained above. Such flexibility for synthesizing an appropriate design greatly enhances the attractiveness of this device as a vibration engineering solution.

Finally, it is desirable to be able to extrapolate the parameters of an absorber designed for a particular load level to another. The load effect is illuminated by the ratio of the stiffness crossing position to tuned absorber displacement, or u/v, which can be expressed as ek_2/p. This ratio indicates that a change in load magnitude can be compensated by a proportional change in the stiffness crossing point. The suppression zone of the modified system is the same as the original one. This guideline is a means of extending a reference configuration to different load levels.

6. Conclusions

The piecewise linear absorber is potentially a popular choice as there are a wide range of materials available for developing appropriate practical applications. Furthermore, designers are already well acquainted with the material performance and fabrication requirements of linear spring design.

The general behaviour of the piecewise linear absorber has been reviewed, in which it is stressed that the free vibration of the absorber mass alone is a major determinant of system response. The number of stiffness crossings for the absorber spring has been examined, with indicative results showing that there are four stiffness crossings per load cycle, which is in line with work in the literature based on assumed crossing frequencies.

The width of the suppression zone has been analyzed through the effects of the stiffness ratio, crossing position and natural frequency ratio, under the condition of harmonic loading. A consistent trend discovered is that a hardening absorber with a low crossing position yields a significantly higher bandwidth than the corresponding linear one. The improvement increases as the trough frequency departs from the structure natural frequency. For a mass ratio of 0.1, it is shown that about a 40% higher bandwidth is possible at a reduced frequency of 1.19. The benefits of a softening absorber is not so definite, even though wide bandwidth solutions have been found. These inevitably exhibit some instability behaviour in the suppression zone. Hopefully, ongoing work would rectify the situation.

This paper has shown that it is feasible to develop a piecewise linear absorber to deliver an excellent attenuation performance. Useful guidelines to aid designers in picking absorber parameters have been synthesized. To fully harness the potential of this concept, an optimization study is planned to methodologically probe the best configurations and to include other designs aspects such as static displacement and stiffness asymmetry.

Appendix

Some matrices and vectors in Equation (5) in the text are given below.

$$\mathbf{S} = \frac{\mathrm{d}\mathbf{f}(\mathbf{y}_0)}{\mathrm{d}\mathbf{y}} \tag{A1}$$

can be readily evaluated through the use of the step function

$$\boldsymbol{\varepsilon} = -\lambda_0^2\mathbf{M}\mathbf{y}_0'' - \lambda_0\mathbf{C}\mathbf{y}_0' - \mathbf{f}(\mathbf{y}_0) + \mathbf{p}(\theta), \tag{A2}$$

$$\mathbf{q} = (-2\lambda_0\mathbf{M}\mathbf{y}_0'' - \mathbf{C}\mathbf{y}_0'). \tag{A3}$$

For the Galerkin approximation

$$\mathbf{H} = \begin{bmatrix} \mathbf{h}^T & \mathbf{0} \\ \mathbf{0} & \mathbf{h}^T \end{bmatrix}, \tag{A4}$$

$$\mathbf{h}^T = [\cos j\theta, \ldots, \sin j\theta, \ldots] \quad (j = 1 \ldots n), \tag{A5}$$

$$\Delta\mathbf{y} = \mathbf{H}\Delta\mathbf{z}, \quad \delta(\Delta\mathbf{y}) = \mathbf{H}\delta(\Delta\mathbf{z}), \tag{A6}$$

$$\mathbf{y}' = \mathbf{H}'\mathbf{z}, \quad \mathbf{y}'' = \mathbf{H}''\mathbf{z}, \quad \Delta\mathbf{y}' = \mathbf{H}'\Delta\mathbf{z}, \quad \Delta\mathbf{y}'' = \mathbf{H}''\Delta\mathbf{z}, \tag{A7}$$

where δ represents variation. Carrying out the Galerkin step by making use of Equations (A6, A7) in Equation (5) and integrating over 2π,

$$\int_0^{2\pi} \delta(\Delta\mathbf{y}^T)(\lambda_0^2\mathbf{M}\Delta\mathbf{y}'' + \lambda_0\mathbf{C}\Delta\mathbf{y}' + \mathbf{S}\Delta\mathbf{y})\,\mathrm{d}\theta = \int_0^{2\pi} \delta(\Delta\mathbf{y}^T)(\boldsymbol{\varepsilon} + \mathbf{q}\Delta\lambda)\,\mathrm{d}\theta, \tag{A8}$$

yields Equation (9), with

$$\mathbf{A} = \int_0^{2\pi} \mathbf{H}^T(\lambda_0^2\mathbf{M}\mathbf{H}'' + \lambda_0\mathbf{C}\mathbf{H}' + \mathbf{S}\mathbf{H})\,\mathrm{d}\theta, \tag{A9}$$

$$\bar{\boldsymbol{\varepsilon}} = \int_0^{2\pi} \mathbf{H}^T\boldsymbol{\varepsilon}\,\mathrm{d}\theta, \tag{A10}$$

$$\bar{\mathbf{q}} = \int_0^{2\pi} \mathbf{H}^T\mathbf{q}\,\mathrm{d}\theta. \tag{A11}$$

For Equation (11)

$$\mathbf{D} = \begin{bmatrix} \mathbf{O} & \mathbf{M} \\ \mathbf{M} & \mathbf{C} \end{bmatrix}, \quad \mathbf{G} = \begin{bmatrix} -\mathbf{M} & \mathbf{O} \\ \mathbf{O} & \mathbf{K} \end{bmatrix}, \quad \mathbf{K} = \begin{bmatrix} k_1 + k_e & -k_e \\ -k_e & k_e \end{bmatrix}, \tag{A12}$$

$$\mathbf{p_d} = [0, 0, p, 0]^T, \tag{A13}$$

$$\mathbf{p_s} = y_e(k_2 - k_d)[0, 0, 1, -1]^T, \tag{A14}$$

$$k_e = \begin{cases} k_d \\ k_2 \\ k_d \end{cases}, \quad y_e = \begin{cases} e & y > e, \\ 0 & -e \le y \le e \\ e & y < -e, \end{cases} \tag{A15}$$

$\mathbf{B}$ and $\mathbf{E}(t)$ are based on the eigenvalues s_1, s_2, and eigenvectors $\mathbf{b}_1$, $\mathbf{b}_2$ of the eigenvalue problem

$$s\mathbf{D}\mathbf{v} = \mathbf{G}\mathbf{v}. \tag{A16}$$

Note that the remaining two eigenvalues and eigenvectors are complex conjugate of the above ones.

$$I = \sqrt{-1}, \quad s_j = \xi_j + I\rho_j, \quad \mathbf{b}_j = \mathbf{b}_{rj} + I\mathbf{b}_{ij}, \quad 1 = \mathbf{b}_j^T\mathbf{D}\mathbf{b}_j \quad (j = 1 \ldots 2), \tag{A17}$$

$$\mathbf{B} = [\mathbf{b}_{r1}, \mathbf{b}_{r2}, -\mathbf{b}_{i1}, -\mathbf{b}_{i2}], \tag{A18}$$

$$\mathbf{E}(t) = \begin{bmatrix} \mathbf{E}_r & -\mathbf{E}_i \\ \mathbf{E}_i & \mathbf{E}_r \end{bmatrix}, \tag{A19}$$

$$\mathbf{E}_r = \mathrm{diag}[\exp(-\xi_j t)\cos(\rho_j t)] \quad (j = 1 \ldots 2), \tag{A20}$$

$$\mathbf{E}_i = \mathrm{diag}[-\exp(-\xi_j t)\sin(\rho_j t)] \quad (j = 1 \ldots 2). \tag{A21}$$

The term $\boldsymbol{\mu}(t)\boldsymbol{\phi}$ is the steady-state solution and is most conveniently found by

$$\mathbf{K_d} = -\lambda^2\mathbf{M} + I\lambda\mathbf{C} + \mathbf{K}, \tag{A22}$$

$$\bar{\mathbf{p}} = [p, 0]^T, \tag{A23}$$

$$\mathbf{a} = \mathbf{K_d}^{-1}\bar{\mathbf{p}}, \tag{A24}$$

$$\mathbf{a} = \mathbf{a}_r + I\mathbf{a}_i, \tag{A25}$$

$$\boldsymbol{\mu}(t) = \begin{bmatrix} -\lambda\mathbf{a}_r\sin(\lambda t) & -\lambda\mathbf{a}_i\cos(\lambda t) & -\lambda\mathbf{a}_r\cos(\lambda t) & \lambda\mathbf{a}_i\sin(\lambda t) \\ \mathbf{a}_r\cos(\lambda t) & -\mathbf{a}_i\sin(\lambda t) & -\mathbf{a}_r\sin(\lambda t) & -\mathbf{a}_i\cos(\lambda t) \end{bmatrix}, \tag{A26}$$

$$\boldsymbol{\mu}_0 = \boldsymbol{\mu}(t = 0), \tag{A27}$$

$$\boldsymbol{\phi} = [\cos\phi, \cos\phi, \sin\phi, \sin\phi]^T, \tag{A28}$$

$$\bar{\boldsymbol{\phi}} = [-\sin\phi, -\sin\phi, \cos\phi, \cos\phi]^T, \tag{A29}$$

$$\mathbf{v}_s = [0, 0, 0, -y_e(k_2 - k_d)/k_d]^T, \tag{A30}$$

$$\mathbf{T} = \mathrm{diag}[\bar{\mathbf{T}}, \bar{\mathbf{T}}], \quad \bar{\mathbf{T}} = \begin{bmatrix} 1 & 0 \\ -1 & 1 \end{bmatrix}. \tag{A31}$$

References

1. Roberson, R. E., 'Synthesis of a nonlinear dynamic vibration absorber', *Journal of the Franklin Institute* **254**, 1952, 205–220.
2. Arnold, F. R., 'Steady state behaviour of systems provided with nonlinear dynamic vibration absorbers', *Journal of Applied Mechanics* **22**, 1955, 487–492.
3. Miller, H. M. and Gartner, J. R., 'Tunable nonlinear vibration absorber', American Society of Mechanical Engineers, Paper No. 75-Det-9, 1975.
4. Hunt, J. B. and Nissen, J. C., 'The broadband dynamic vibration absorber', *Journal of Sound and Vibration* **83**(4), 1982, 573–578.
5. Nissen, J. C., Popp, K., and Schmalhorst, B., 'Optimization of non-linear dynamic vibration absorber', *Journal of Sound and Vibration* **99**(1), 1985, 149–154.
6. Rice, H. J. and McCraith, J. R., 'Practical non-linear vibration absorber design', *Journal of Sound and Vibration* **116**(3), 1987, 545–559.
7. Natsiavas, S., 'Regular and chaotic response of vibration absorbers with elastic stops', in *Nonlinear Vibrations*, ASME DE-Vol. 50/AMD-Vol. 144, 1992, pp. 15–20.
8. Natsiavas, S., 'Dynamics of multiple-degree-of-freedom oscillators with colliding components', *Journal of Sound and Vibration* **165**(3), 1993, 439–453.
9. SAE Spring Committee, *Spring Design Manual*, Society of Automotive Engineers, Warrendale, 1996.
10. Lau, S. L., Cheung, Y. K., and Wu, S. Y., 'Nonlinear vibration of thin elastic plates', *Journal of Applied Mechanics* **51**, 1984, 837–843.
11. Pun, D., Lau, S. L., and Liu, Y. B., 'Internal resonance of an L-shaped beam with a limit stop: Part I, Free vibration', *Journal of Sound and Vibration* **193**(5), 1996, 1023–1035.
12. Pun, D., Lau, S. L., and Liu, Y. B., 'Internal resonance of an L-shaped beam with a limit stop: Part II, Forced vibration', *Journal of Sound and Vibration* **193**(5), 1996, 1037–1047.
13. Lau, S. L. and Zhang, W. S., 'Nonlinear vibrations of piecewise-linear systems by incremental harmonic balance method', *Journal of Applied Mechanics* **59**, 1992, 153–160.
14. Cheung, Y. K., Chen, S. H., and Lau, S. L., 'Application of the incremental harmonic balance method to cubic nonlinearity systems', *Journal of Sound and Vibration* **140**(2), 1990, 273–286.
15. Masri, S. F. and Caughey, T. K., 'On the stability of the impact damper', *Journal of Applied Mechanics* **33**, *Transactions ASME* **88**, Series E, 1966, 586–592.
16. Pun, D., Lau, S. L., and Cao, D. Q., 'Forced vibration of a multidegree impact vibrator', *Journal of Sound and Vibration* **213**(3), 1998, 447–466.